RSC Advances

PAPER

View Article Online
View Journal | View Issue

Cite this: *RSC Adv.*, 2014, **4**, 40930

Published on 18 August 2014. Downloaded by University of Queensland on 1/21/2019 6:03:50 AM.

# Complexing agent study *via* computational chemistry for environmentally friendly silver electrodeposition and the application of a silver deposit†

Anmin Liu,[a] Xuefeng Ren,[a] Bo Wang,[ab] Jie Zhang,[a] Peixia Yang,[a] Jinqiu Zhang[a] and Maozhong An*[a]

Received 17th June 2014
Accepted 15th August 2014

DOI: 10.1039/c4ra05869k

www.rsc.org/advances

In this paper, we introduce a new environmentally friendly silver electroplating bath, employing 5,5-dimethylhydantoin (DMH) and nicotinic acid (NA) as complexing agents, based on the prediction of computational chemistry. An excellent silver electrodeposit with properties suitable for application in electronics packaging was obtained from the newly developed silver electroplating bath, and the electroplating bath is simple and stable. Moreover, the silver(I)-complexes in this bath possessed good complex stability. As a consequence, mirror-bright silver electrodeposits on copper substrates with excellent leveling capability, smooth and compact morphologies, high purity and conductivity, as well as excellent welding property could be realized by adopting this unique bath. Based on the performances of the plating bath and silver deposit, the introduced silver plating bath is a promising candidate for silver electrodeposition applied in microelectronics to replace the conventional cyanide silver electroplating baths.

## 1. Introduction

Silver-based materials are widely used in microelectronics owing to their excellent physico-chemical properties, good corrosion resistance, high bulk conductivity, excellent welding performance and beautiful features.[1–6] Successfully obtaining compact, smooth, and adhesive silver deposits for electronics remains an important technological goal. Ever since the first patent described in 1840, silver deposits have usually been electrodeposited in cyanide baths, which offer the most consistent deposit quality at the lowest cost.[7–11] Unfortunately, cyanide is one of the most toxic chemicals available, and therefore its use carries an extremely high risk to human health and to the environment.[12] Furthermore, disposal of the exhausted plating bath and wastewater treatment are becoming increasingly difficult and expensive, rendering this approach highly unattractive from an industrial perspective.[13,14]

In order to overcome these challenges, a number of cyanide-free silver plating bath configurations have been investigated over recent years. The most notable cyanide-free silver plating bath involves a thiosulfate-based formulation, and has proven to be the most successful approach so far among several investigated inorganic complexes. Mirror-bright silver deposits with low porosity and high anti-tarnish capabilities were obtained, with the silver electrodeposits obtained from the sodium thiosulfate solutions possessing noticeably smooth surfaces.[15–18] While thiosulfate systems have found to not only be inherently safer and environmentally friendlier than cyanide systems, they also provide better deposit thickness distributions on complex-shaped objects. However, the thiosulfates were found to be unstable due to the disproportionation of free thiosulfate ions to generate colloidal sulphur. The resulting colloidal sulphur may then significantly compromise the anti-tarnish capability, conductivity, or other important properties of the silver deposits, leaving it impractical for commercial purposes.

Therefore, in order to overcome these inherent limitations of thiosulfate and to successfully develop cyanide-free silver electroplating systems, alternative complexing agents, especially organic compounds with excellent stability and environmental friendliness, require investigation. A number of attempts have been made in the past few years to develop cyanide-free silver plating baths. During these attempts, the complexing agents for silver electroplating were widely investigated owing to their important role in the electroplating process. As a result, new complexing agents for cyanide-free silver plating baths, such as uracil,[19] ammonia,[20,21] thiourea,[22] HEDTA,[23] 2-

[a]State Key Laboratory of Urban Water Resource and Environment, School of Chemical Engineering and Technology, Harbin Institute of Technology, Harbin, 150001, China. E-mail: mzan@hit.edu.cn; Fax: +86-451-86418616; Tel: +86-451-86418616

[b]Faculty of Engineering, Architecture and Information Technology, School of Chemical Engineering, The University of Queensland, St Lucia, Brisbane, QLD 4072, Australia

† Electronic supplementary information (ESI) available. See DOI: 10.1039/c4ra05869k



This journal is © The Royal Society of Chemistry 2014

Published on 18 August 2014. Downloaded by University of Queensland on 1/21/2019 6:03:50 AM.

hydroxypyridine,[24,25] and ionic liquids[12,26] were proposed. However, except for a few successful cases, most of these baths still suffer from problems of instability, sensitivity to temperature or light, and relatively high toxicity and cost, as well as low deposit quality, including severe adhesion and inferior morphologies. Consequently, more efforts need to be directed toward this technology to find a comparable and environmental friendly alternative to cyanide baths.

However, researching new complexing agents through experimentation is expensive, both in time and resources. Therefore, time-saving techniques to choose or design better complexing agents for silver electroplating are urgently needed. Computational chemistry is an emerging area of research for the modeling of small chemical and biological systems in order to understand and predict their behaviors at the molecular level.[27–29] Quantum chemical calculations[30–35] and molecular dynamic (MD) simulations[36–38] have become useful methods to study many natural systems in pharmacology,[39] chemistry,[40–45] and biology.[46,47] Moreover, the bonding interactions between ions and complexing agents can be studied by computational chemistry.[48–51]

In addition to the coordinating ability with metal ions in solution, complexing agents can adsorb on metal surfaces, due to their oxygen and nitrogen containing components. MD simulation is a convenient way to study the interactions between molecules and interfaces,[52–55] and has been used to simulate the adsorption behaviours of organic molecules,[56,57] electroplating additives,[58,59] and corrosion inhibitors[60,61] on metal surfaces.

In this work, 5,5-dimethylhydantoin (DMH) was selected as a complexing agent for silver electroplating. Compared to those reported complexing agents used for cyanide-free silver electroplating baths, hydantoin,[62] a heterocyclic structure organic molecule with good solubility and stability in alkaline solution in a large temperature range, and its derivatives act as more stable complexing agents for silver(I)[63] and other metal ions.[64,65] Among a series of substituted hydantoins, DMH is the most commercially available as a complexing agent for metal electroplating at high current density ranges and high temperatures.[66] Despite this progress, no commercial process utilizing this silver plating bath has yet been reported, due to the disadvantage of the bath or the deposit performance.

In order to improve the performance of the DMH-based silver electroplating bath, we tested auxiliary complexing agents usually used for the DMH-based cyanide-free silver electroplating bath. Quantum chemical calculations were employed to investigate the electronic properties and orbital information of the studied complexing agents. The interactions between the possible complexing agents and the metal surface were studied by MD simulations. The performances of the silver deposit and DMH-based silver electroplating bath were determined by experiment. Based on these studies, a mirror-bright silver deposit with excellent leveling capability, smooth and compact morphologies, and high purity and conductivity, as well as excellent welding properties could be obtained from the studied bath without any additives.

# 2. Experimental

## 2.1 Quantum chemical calculations and MD simulations

Quantum chemical calculations were performed by the $DMol^3$ module in Materials Studio (from Accelrys Inc.). Some electronic properties and orbital information of the studied complexing agents were calculated by DFT methods using the BLYP exchange–correlation functional. 12 complexing agents with oxygen and nitrogen containing heterocyclic structures or oxygen and nitrogen containing chain organic compounds were selected as potential complexing agents to be investigated.

MD simulations of the adsorption interactions between the complexing agents and the copper and silver surfaces were carried out in a simulation box with periodic boundary conditions using Materials Studio. The box consisted of a silver or copper surface (cleaved along the (111) plane, with a volume of 2.600 nm × 2.600 nm × 1.179 nm of Ag and 2.300 nm × 2.300 nm × 1.043 nm of Cu, respectively.), a liquid phase, and a vacuum layer of 1 nm height. The liquid phase was water molecules with a density of 1 g $cm^{-3}$ and containing 3 complexing agent molecules. The MD simulations were performed at 328 K, utilizing a NVT ensemble and the COMPASS force field, with a time step of 1 fs and a simulation time of 200 ps.

The interaction energy between the metal surface and organic molecules was calculated using eqn (1).

$$E_{\text{Interaction}} = E_{\text{Total}} - E_{\text{Metal}} - E_{\text{Agents}} \tag{1}$$

where $E_{\text{Total}}$ was the total energy of the copper or silver crystal together with the adsorbed complexing agents and $E_{\text{Metal}}$ and $E_{\text{Agents}}$ were the total energy of the copper or silver crystal and free agents, respectively. The adsorption energy was the negative value of the interaction energy.

## 2.2 Measurements and apparatus

Silver electroplating experiments were conducted under galvanostatic conditions in a cell, employing a silver anode and a copper substrate. All solutions in this work were prepared using analytical grade reagents and deionized water. $AgNO_3$ was chosen as the source of silver ions, and a silver anode with a distance of 5–15 cm to the working electrode, was used to make up for the consumption of silver ions during the electrodeposition. The silver plating bath was prepared by adding $AgNO_3$ solution into a solution containing DMH, NA, and $K_2CO_3$, and the pH value of the bath was adjusted to 10.0–14.0 with KOH solution.

The electrochemical measurements were performed in a three-electrode cell using a potentiostat/galvanostat (PARSTAT2273 Electrochemical Integrated Test System, Princeton Applied Research) at 328 K. A glassy carbon electrode (GCE) with a diameter of 3 mm was employed as the working electrode (WE). The counter electrode (CE) was a platinum plate with an area of 1 $cm^2$. A mercuric oxide electrode (Hg/HgO) was used as the reference electrode (RE). The potential scan was initiated at an open circuit potential from −1.30 V to 1.15 V, with a sweep rate of 10 mV $s^{-1}$ at 328 K.

Published on 18 August 2014. Downloaded by University of Queensland on 1/21/2019 6:03:50 AM.

A gloss meter was employed to measure the glossiness of the silver deposits. Field emission scanning electron microscopy (FESEM, XL30S-FEG, FEI) was used to study the surface morphologies of the silver deposits. An atomic force microscope (AFM) was employed to study the surface roughness of the silver deposits. The AFM analysis was carried out with a Dimension Icon (Bruker), working in contact mode with silicon nitride cantilevers. The micro-hardness of the deposit was measured by a micro-hardness tester. The investigation of impurities in the deposits was performed by X-ray photoelectron spectroscopy (XPS). The XPS spectra were taken using a PHI 5700 ESCA System (Physic Electronics, USA) operating at room temperature. The excitation source was Al Kα radiation (photoelectron energy, 1486.6 eV), and the photoelectrons were detected with a hemispherical analyzer. A contact resistance tester was present to test the contact resistance of the silver deposits. The welding property measurements were performed on an Ultrasonic bonder (Ultrasonic Technology Co., Ltd).

# 3. Results and discussion

## 3.1 Quantum chemical calculations and MD simulations

The oxygen and nitrogen species in organic molecules ensure a firm coordination with metal ions ($Ag^+$), as well as adsorption on metal surfaces (Cu or Ag). Twelve different possible complexing agents forming silver(I)-complexes were studied, based on their molecular structures.

Quantum chemical calculations based on DFT principles were employed to study the electronic properties and orbital information of each agent. According to the frontier molecular orbital theory, the energy of the highest occupied molecular orbital (HOMO) and of the lowest unoccupied molecular orbital (LUMO) are often associated with the electron donating ability and electron accepting ability of molecules. Higher values of $E_{HOMO}$ (energy of HOMO) and lower values of $E_{LUMO}$ (energy of LUMO) indicate a tendency of a molecule to donate and accept electrons, respectively.

Fig. 1 exhibits the distribution of the HOMO and electron cloud densities of the studied complexing agents. The presence of nitrogen and oxygen atoms gave significant contributions to the HOMO, expect in the case of HEDTA. This was due to the electron donating properties of the nitrogen and oxygen atoms, resulting in the ability to form silver(I)-complex coordinated bonds.

The distribution of LUMO is displayed in Fig. 2. Molecules (a)–(h) showed a similar localization of the LUMO and electron cloud densities, indicating similar electronic properties and electron accepting abilities. In addition to the localization of the molecular orbitals, $E_{HOMO}$ and $E_{LUMO}$, and their difference ($\Delta E$) are useful tools to characterize the electronic properties and adsorption behaviors of each agent.

$E_{HOMO}$ and $E_{LUMO}$, along with $\Delta E$, are important molecular electronic properties that determine the behavior and adsorption properties of various complexing agents. A schematic depiction of these values based on the frontier molecular orbitals is presented in Fig. 3. Structures (a), (e), (g), and (h) with similar, relatively high $E_{HOMO}$ values of −5.912 eV, −5.922 eV, −5.892 eV, and −5.920 eV, respectively, are possibly good complexing agents owing to their propensity to donate electrons to $Ag^+$ and to form coordinated molecular structures. The difference between the frontier molecular orbitals of these structures was mainly in $E_{LUMO}$. This corresponds to varying $\Delta E$ values, leading to different stabilities of the complexing agent adsorption layers on the metal surface.[67,68] With the smallest $\Delta E$ calculated for structures (a), (e), (g), and (h), this suggests a more effective adsorption of NA on the metal surfaces.

MD simulations were performed to study the adsorption behaviors of all the studied complexing agents on Cu (111) and Ag (111) surfaces, with the results from the DMH simulations included in this paper and the remainder in the ESI† due to space limitations. The adsorption behaviors of DMH on Cu (111) and Ag (111) surfaces are shown in Fig. 4 and 5, respectively. Fig. 4(a) and 5(a) show the initial configuration of the MD simulation boxes. Fig. 4(b) and 5(b) show the final equilibrium configuration of the MD simulation boxes at 328 K, with a time step of 1 fs and a simulation time of 200 ps. Fig. 4(c) and 5(c) display the top view of the final equilibrium configuration of the simulation box. The interface absorption structures of DMH on Cu and Ag surfaces are shown in Fig. 4(f) and 5(f), respectively. Fig. 4(d), 5(d), 4(e), and 5(e) show the energy and temperature fluctuation curves of the MD simulations. These plots indicate that the simulation systems were already at equilibrium by their completion.

The adsorption energies and MD simulation boxes of all the other studied complexing agents are summarized in Table 1 and Fig. S1–S22 (ESI†), respectively.

The main conclusions drawn from these simulations highlight that structures (a), (b), (e), (f), (g), (h), (i), (k), and (l) could adsorb on the metal surfaces with higher energies (with an adsorption energy on Cu (111) greater than 250 kJ $mol^{-1}$, and greater than 190 kJ $mol^{-1}$ on the Ag (111) surface). Moreover, as shown in Fig. S1–S22 (ESI†), DMH, 2-hydroxypyridine, pyridine, imidazole, NA, nicotinamide, succinimide, and uracil rings were virtually parallel to the copper and silver surfaces, suggesting effective adsorptions on the metal surfaces. The results of the MD simulations showed that 2-hydroxypyridine, pyridine, imidazole, NA, nicotinamide, succinimide, uracil, HEDTA, and triethylenetetramine could adsorb on the copper and silver surfaces strongly, leading to a higher inhibited effect for silver electrodeposition on the copper and silver surfaces.

Based on the quantum chemical calculations and MD simulations, with similar, relatively high $E_{HOMO}$ values and effective adsorptions on the metal surfaces, 2-hydroxypyridine, NA, and uracil could be used as auxiliary complexing agents for the DMH-based cyanide-free silver electroplating bath, because of their strong electron donating abilities and high adsorption energies. Combined with its other advantages, such as low cost, good solubility, and stability in alkaline solution in a large temperature range, NA was selected as an auxiliary complexing agent for the introduced DMH-based silver electroplating bath in the present paper. Electrochemical measurements and silver electroplating were carried out to further confirm these predictions.

 This journal is © The Royal Society of Chemistry 2014

Published on 18 August 2014. Downloaded by University of Queensland on 1/21/2019 6:03:50 AM.

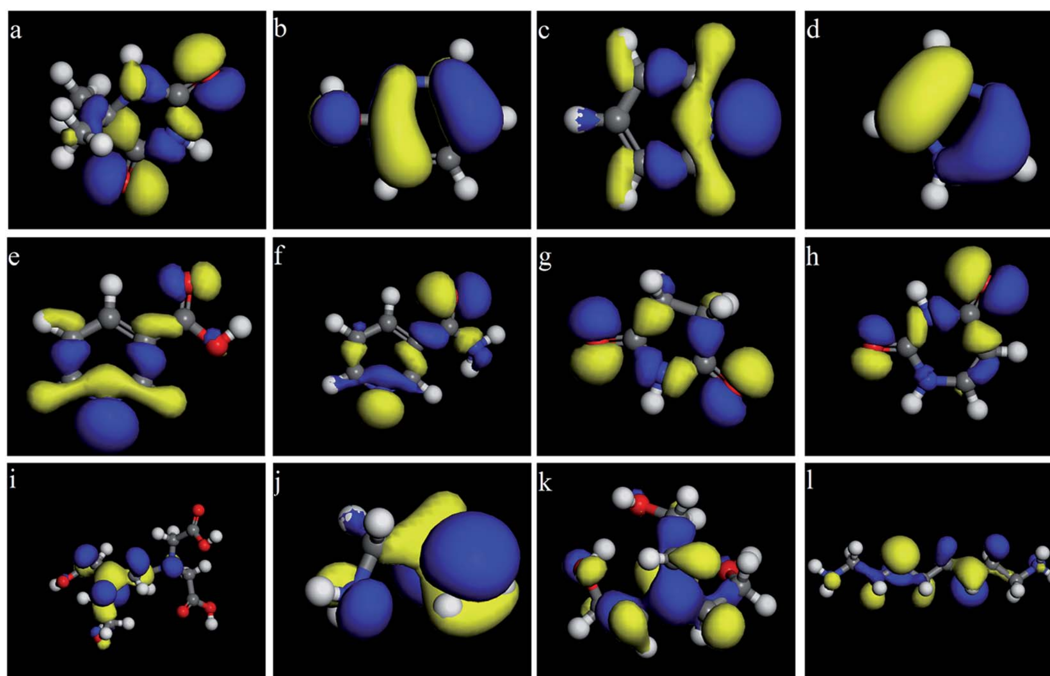


Fig. 1 Localization of the highest occupied molecular orbital (HOMO) of (a) DMH, (b) 2-hydroxypyridine, (c) pyridine, (d) imidazole, (e) NA, (f) nicotinamide, (g) succinimide, (h) uracil, (i) HEDTA, (j) ethylenediamine, (k) triethanolamine, and (l) triethylenetetramine.

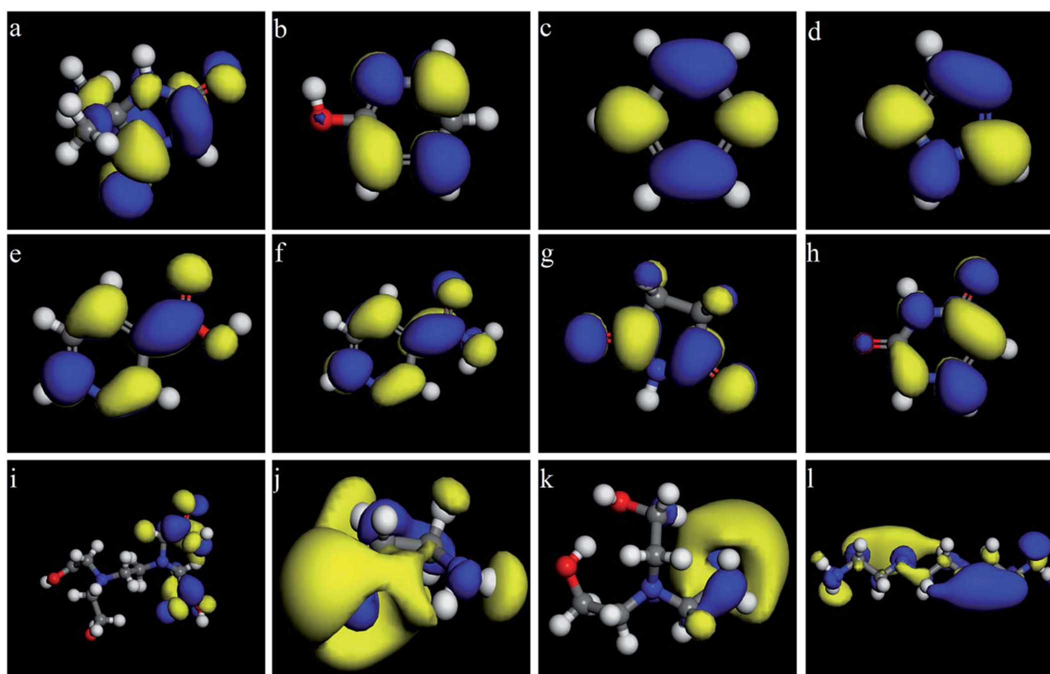


Fig. 2 Localization of the lowest unoccupied molecular orbital (LUMO) of (a) DMH, (b) 2-hydroxypyridine, (c) pyridine, (d) imidazole, (e) NA, (f) nicotinamide, (g) succinimide, (h) uracil, (i) HEDTA, (j) ethylenediamine, (k) triethanolamine, and (l) triethylenetetramine.

### 3.2 Stability of the plating bath

The stability of the employed silver plating bath, particularly in the case of extreme temperature (high or low) conditions, is a very important consideration for practical applications. For these investigations, the plating bath was heated at 373 K for 15 minutes, followed by rapid cooling back to room temperature, in order to gauge the temperature stability. No changes to the bath were detected, and the mirror-bright silver deposits could still be obtained from the bath after the aforementioned thermal experiments. These observations indicate that the

Published on 18 August 2014. Downloaded by University of Queensland on 1/21/2019 6:03:50 AM.

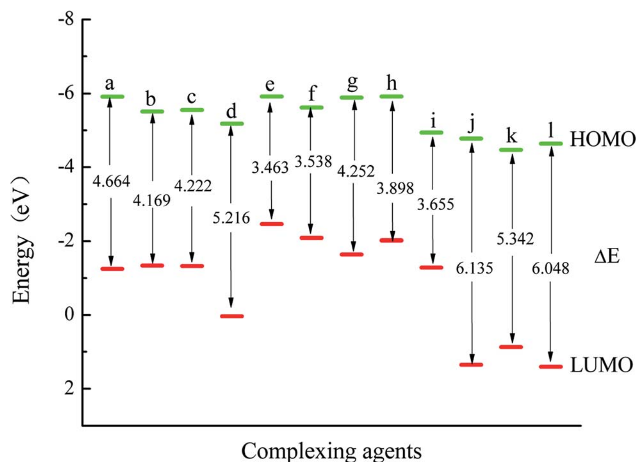


Fig. 3 Schematic diagrams of the frontier molecular orbitals of (a) DMH, (b) 2-hydroxypyridine, (c) pyridine, (d) imidazole, (e) NA, (f) nicotinamide, (g) succinimide, (h) uracil, (i) HEDTA, (j) ethylenediamine, (k) triethanolamine, and (l) triethylenetetramine, and the calculated $E$ (eV).

silver plating bath utilized possessed excellent thermal stability in the investigated range. Furthermore, after 12 months of bath storage, no precipitates or bath discoloration were visually observed, indicating good stability over this long time period.

In order to further investigate the stability of the bath, cyclic voltammetry was used to study the electrochemical behavior from inserting a GCE into the bath. The potential scan of the cyclic voltammetry started at an open circuit potential, with a sweep rate of 10 mV $s^{-1}$ from −1.30 V to 1.15 V. Fig. 6 shows the cyclic voltammograms curves obtained after different electrodeposition times or after storage for different durations of time. As seen in this figure, there was no significant change in the reduction and oxidation peaks of the silver plating baths after different electrodeposition times, or after storage for 10 days, indicating that the silver plating bath possesses good electrochemical stability. Moreover, compared with the cyclic voltammograms of $AgNO_3$ solution displayed in Fig. S23 (ESI†), the silver deposit potential negatively shifted in the presence of the complexing agents. This illustrates that the silver complexes in the introduced bath possessed high complex stability and that DMH, as well as NA, can significantly inhibit the reduction of silver.

In order to further confirm the above conclusions, a displacement reaction was employed. Poorly adhering silver deposits on copper substrates usually result from a displacement reaction occurring between copper and silver(I)-complexes inside the electrolyte before electroplating. Commonly, a thin silver deposit is strike-plated before electrodeposition to overcome this problem; however, if the displacement reaction in the silver plating bath can be avoided, the strike-plating process could become unnecessary. In this experiment, a copper substrate with a removed surface oxide layer was immersed in the silver plating bath. No difference was observed on the copper surface after immersion for 10–15 minutes. Thus, no strike-plating process was necessary to obtain good adherent silver deposits on the copper substrate using the introduced silver plating bath containing DMH and NA as complexing agents.

The current efficiency of the plating bath, tested by a copper coulometer, was nearly 100% in the working current density range. Silver electrodeposition or anodic dissolution without side reactions can also significantly increase the stability of the bath. In consideration of the excellent performance, along with the high stability in a large temperature range, and after long storage times, and in terms of electrodeposition efficiency, the bath possesses practical significance in various fields of application.

### 3.3 Function of silver electroplating

Based on the quantum chemical calculations and MD simulations, DMH and NA were chosen as the complexing agents for the introduced silver plating bath. The optimal technological parameters, such as current density, temperature, and time, were determined by the deposit appearance. Parameters with which mirror-bright and smooth silver deposits were obtained were used for the silver electrodeposition in present work.

After the silver plating onto copper substrates was carried out, mirror-bright silver deposits were obtained from plating baths containing DMH and NA complexing agents. The glossiness of the silver deposits obtained from the plating bath and from the conventional cyanide silver electroplating bath was compared, as listed in Table 2. The glossiness measurements were repeated five times for every deposit.

The glossiness of the silver deposits obtained from the introduced bath was very close to those of the cyanide bath silver deposits. This indicates that the introduced bath could be a promising candidate for electronic packaging, such as for LEDs, which require a glossiness of silver deposits of around 1.0–2.0.

The surface morphology is also a very important consideration for electronic packaging applications. Field emission scanning electron microscopy (FESEM) and atomic force microscopy (AFM) techniques were employed to characterize the surface morphology of the silver deposits. Fig. 7 displays the SEM top view images of the silver deposits obtained from the silver electroplating bath introduced in this work. It can be clearly seen that the silver deposit was smooth and that the corresponding size of grains was less than 100 nm (Fig. 7(b)). These observations are most likely due to using a combination of DMH and NA as the composite complexing agents, which caused an increase in the cathodic polarization and which resulted in smaller grains in the silver deposit. As observed in the cyclic voltammograms displayed in Fig. 6, the onset of the $Ag^+$ reduction reaction was at −0.80 V and the deposition peak was at −0.95 V, with a large polarization of silver, suggesting that DMH and NA can significantly inhibit the reduction of silver, and thereby tiny silver particles can be obtained.

AFM three-dimensional height images of the copper substrate with and without silver deposits are presented in Fig. 8(a) and (b), respectively. The copper substrate clearly has trenches on the surface (Fig. 8(a)), while the silver deposit surface (Fig. 8(b)) shows a relatively smoother morphology. The

 This journal is © The Royal Society of Chemistry 2014

Published on 18 August 2014. Downloaded by University of Queensland on 1/21/2019 6:03:50 AM.

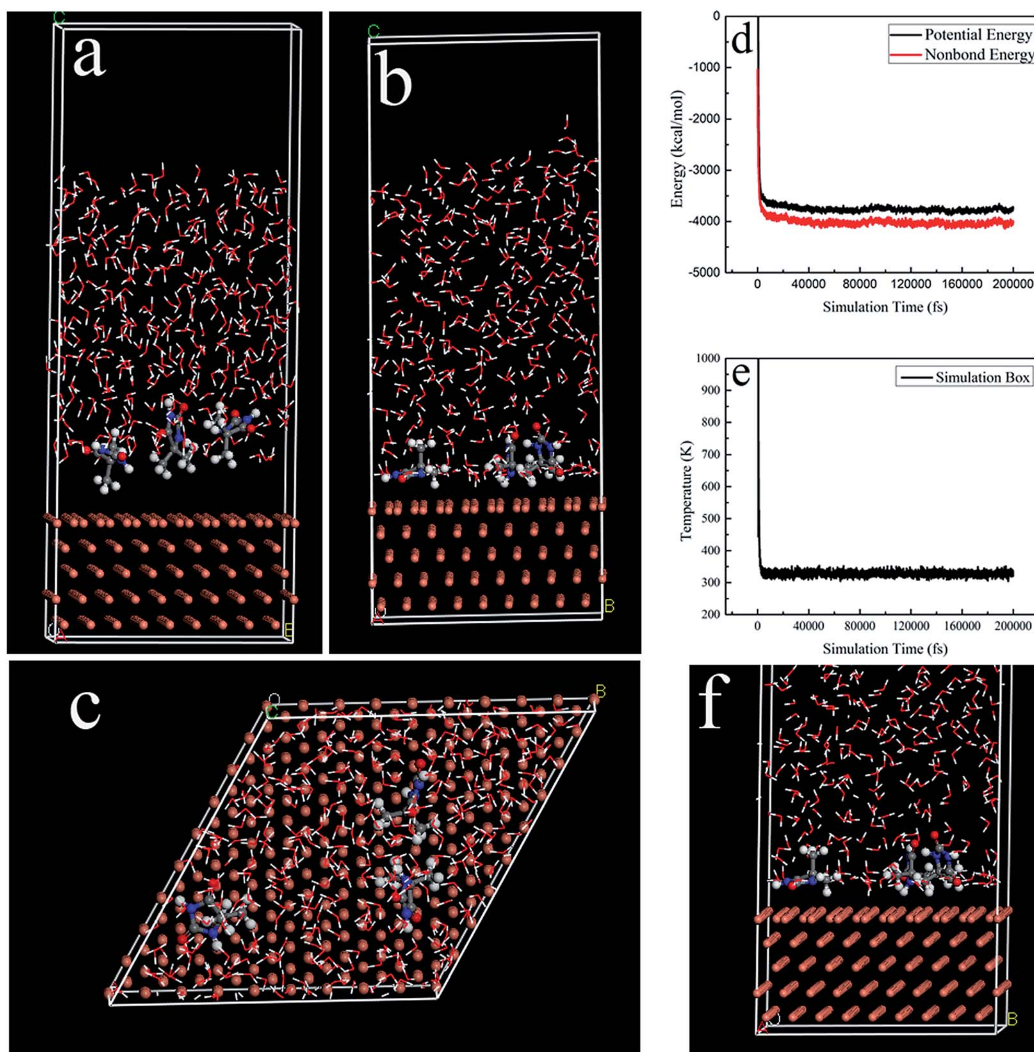


Fig. 4 (a) Initial configuration of the simulation box (DMH visualized by balls and sticks, water molecule visualized by lines). (b) Final equilibrium configuration of the MD simulation box (adsorption behaviors of DMH on the Cu surface). (c) Top view of the final equilibrium configuration of the simulation box. (d) Energy fluctuation curves of the MD simulation. (e) Temperature fluctuation curve of the MD simulation. (f) Interface adsorption structure of DMH on the Cu surface.

trenches almost disappear after the copper surface was electrodeposited with silver. The $R_a$, $R_q$, and $R_{max}$ of the copper surface were 6.64 nm, 8.34 nm and 55.0 nm, respectively. In contrast, the $R_a$, $R_q$ and $R_{max}$ of the silver deposit surface were 4.11 nm, 3.26 nm and 29.2 nm, respectively. It can therefore be concluded from the AFM measurements that the introduced bath for silver plating possessed an excellent levelling capacity.

### 3.4 Micro-hardness of silver deposit

The micro-hardness (HV) influences the service life of the silver deposits and is an important property for its application in microelectronics, aerospace, automotive and jewelry industries. Fig. 9 displays a comparison of the micro-hardness of silver deposits obtained from the introduced bath in this work, a conventional cyanide bath and a conventional hard silver electroplating bath.

The micro-hardness of the silver deposit obtained from the introduced bath without any additives is 68 (HV), close to 70 (HV) for a cyanide bath silver deposit and lower than 120 (HV) for a hard silver deposit. Therefore, the silver deposit obtained from the introduced bath could be processed and welded for electronic packaging applications in a fashion similar to cyanide-based silver deposits. In consideration of the excellent performances in terms of processing and welding, the introduced bath in this work could be applied in microelectronics to replace the conventional cyanide silver electroplating bath.

### 3.5 Purity of silver deposit

Impurities such as complexing agents or additives interfused in the deposits are common in metal electrodeposition and seriously affect the properties and quality of the resulting deposits. For applications in microelectronics, aerospace, automotive,

Published on 18 August 2014. Downloaded by University of Queensland on 1/21/2019 6:03:50 AM.

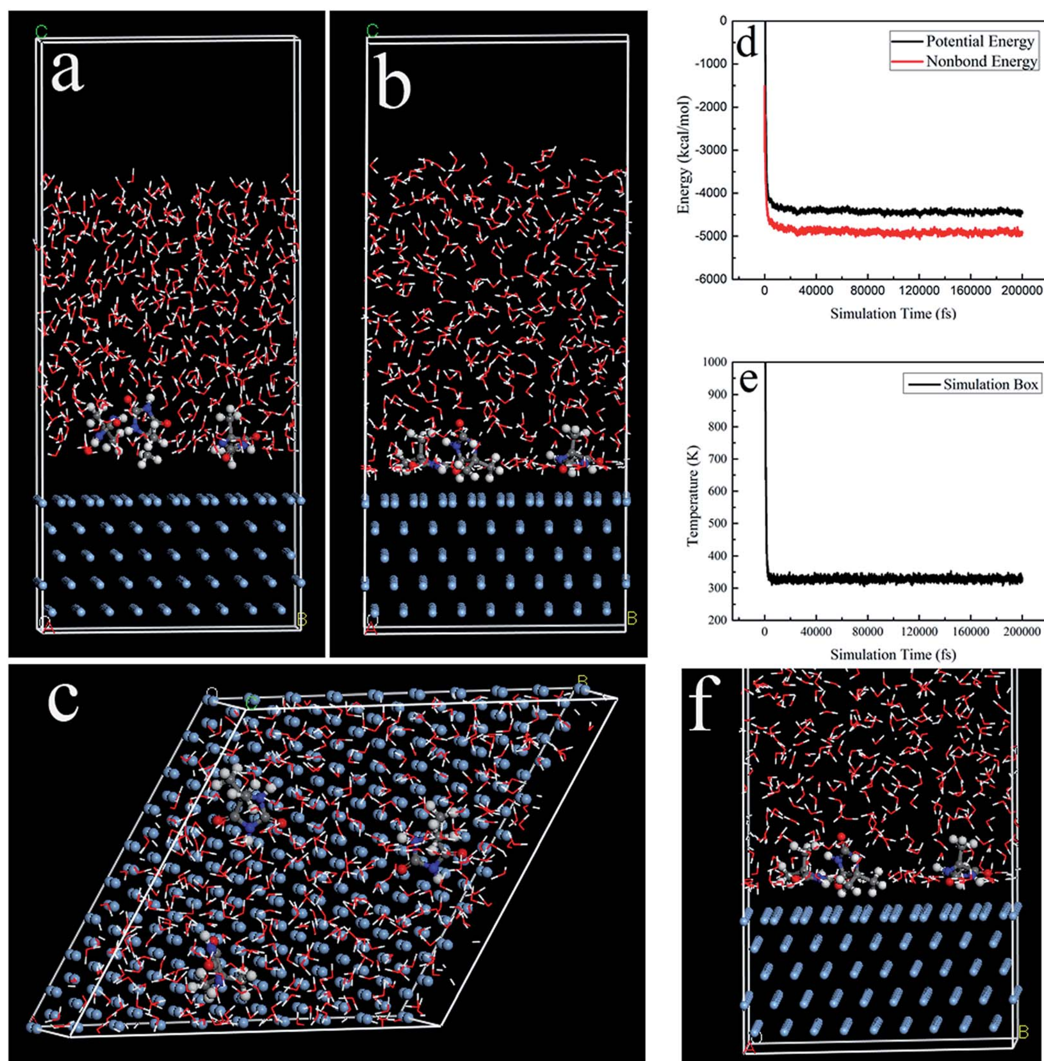


Fig. 5 (a) Initial configuration of the simulation box (DMH visualized by balls and sticks, water molecule visualized by lines). (b) Final equilibrium configuration of the MD simulation box (adsorption behaviors of DMH on the Ag surface). (c) Top view of the final equilibrium configuration of the simulation box. (d) Energy fluctuation curves of the MD simulation. (e) Temperature fluctuation curve of the MD simulation. (f) Interface adsorption structure of DMH on the Ag surface.

Table 1 Adsorption energies of all the studied complexing agents on Cu (111) and Ag (111) surface (unit of kJ $mol^{-1}$)

| | | Cu (111) | Ag (111) |
|---|---|---|---|
| a | DMH | 280.853 | 228.083 |
| b | 2-Hydroxypyridine | 262.090 | 197.080 |
| c | Pyridine | 234.354 | 209.943 |
| d | Imidazole | 196.565 | 155.168 |
| e | NA | 341.474 | 259.066 |
| f | Nicotinamide | 357.929 | 267.830 |
| g | Succinimide | 294.902 | 224.983 |
| h | Uracil | 344.961 | 257.226 |
| i | HEDTA | 383.468 | 303.342 |
| j | Ethylenediamine | 188.086 | 127.467 |
| k | Triethanolamine | 294.839 | 249.504 |
| l | Triethylenetetramine | 365.863 | 216.507 |

and jewelry industries, the anti-tarnish abilities and electrical properties of the silver deposits are severely compromised by impurities. XPS analyses were carried out to examine the composition of the atoms in the silver deposit.

An XPS survey scan was taken over a wide binding energy region from 1.200–1350.000 eV, which indicated the presence of silver, carbon, nitrogen, oxygen, and sulphur species. The binding energy of the C 1s peak at 284.6 eV was used as an internal standard.

Fig. 10 displays the composition of the original surface and a 10.0 nm depth of silver deposit obtained from the DMH and NA silver plating bath. The concentration of atoms at the original surface and at a 10.0 nm depth of silver deposit measured by XPS are shown in Table 3.

Ag, C, N, and O were present on the surface with atomic contents of 54.06 at% (Ag 3d), 34.27 at% (C 1s), 7.74 at% (N 1s), and 3.93 at% (O 1s), but no signals for S 2p, respectively. No

 This journal is © The Royal Society of Chemistry 2014

Published on 18 August 2014. Downloaded by University of Queensland on 1/21/2019 6:03:50 AM.

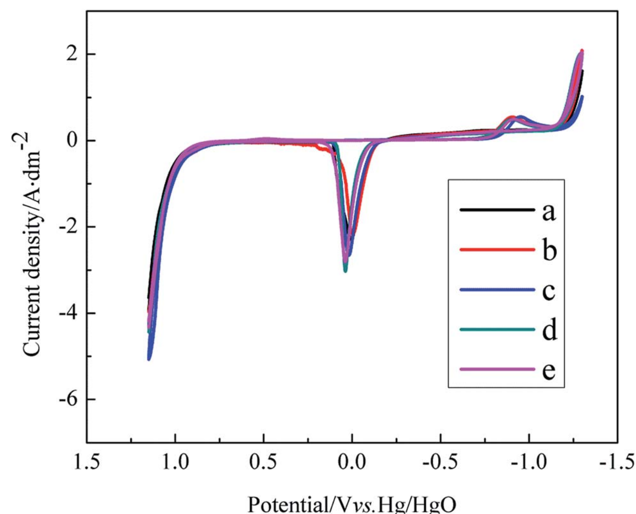


Fig. 6 Cyclic voltammograms of the introduced silver plating bath (a) 40 A h $L^{-1}$ electrodeposition in 45 days, (b) 15 A h $L^{-1}$ electrodeposition in 20 days, (c) 10 A h $L^{-1}$ electrodeposition in 10 days, (d) new prepared bath, (e) stored 10 days without electrodeposition. (A h $L^{-1}$, ampere-hour per liter silver plating bath, indicates the power consumption or the workload of the silver plating bath).

Table 2 Glossiness of silver deposits obtained from different silver electroplating baths

| | Maximum | Minimum | Average | Range |
|---|---|---|---|---|
| Introduced bath | 1.77 | 1.52 | 1.690 | 0.25 |
| Cyanide bath | 1.78 | 1.67 | 1.724 | 0.11 |

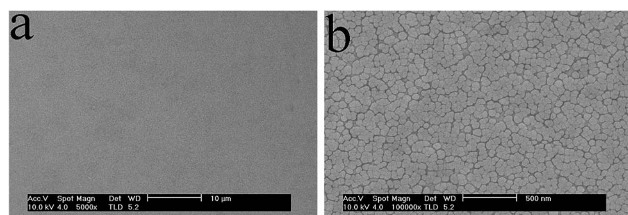


Fig. 7 SEM images of the top views of silver deposits obtained from the silver electroplating bath introduced in this work, (a) 5000 times magnification and (b) 100 000 times magnification.

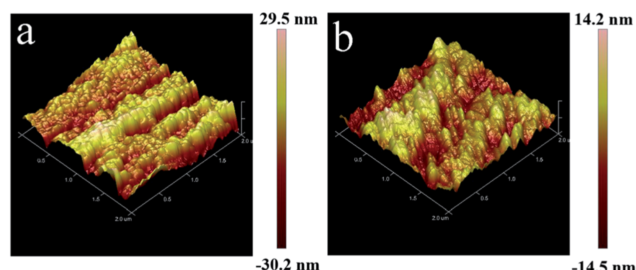


Fig. 8 AFM three-dimensional height images of (a) the polished copper surface and (b) the silver deposit surface.

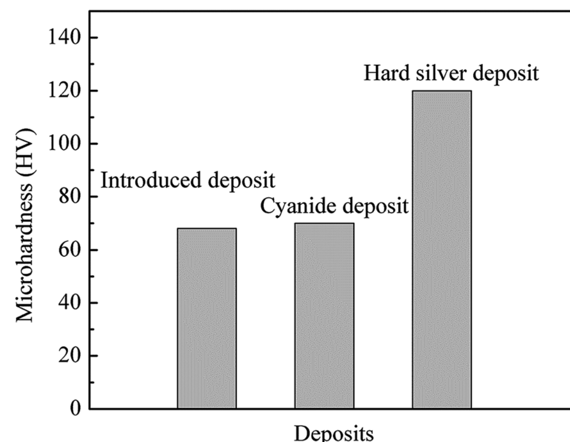


Fig. 9 Micro-hardness of silver deposits obtained from the introduced bath in this work, the conventional cyanide bath and the conventional hard silver electroplating bath.

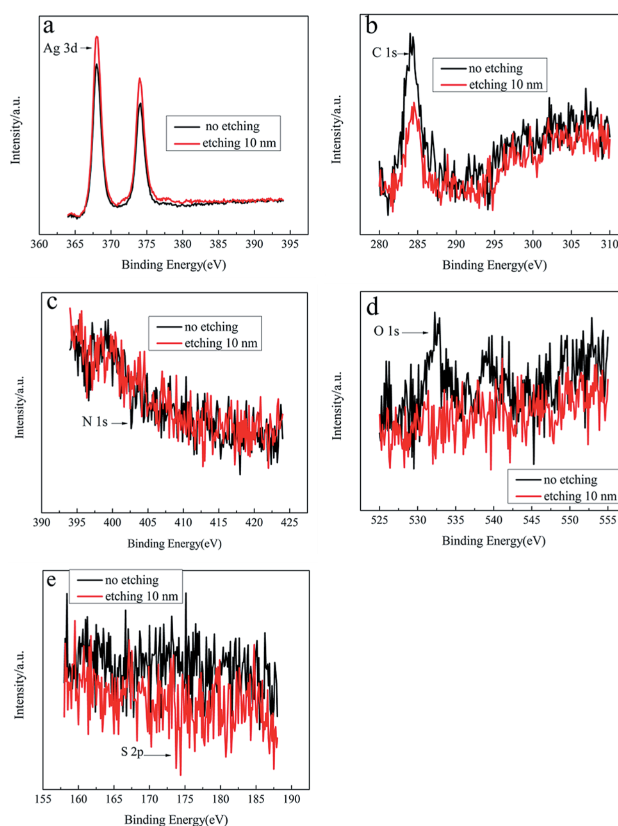


Fig. 10 XPS spectra of the original surface and a 10.0 nm depth of silver deposits. (a) XPS spectra of silver, (b) XPS spectra of carbon, (c) XPS spectra of nitrogen, (d) XPS spectra of oxygen, and (e) XPS spectra of sulfur.

signals for O and S could be detected at a 10.0 nm depth of silver deposit at the sensitivity limit of XPS, indicating that DMH and NA only adsorbed on the surface of silver, while the content of DMH and NA in the bulk silver was very low and the purity of the silver deposit was very high.

Published on 18 August 2014. Downloaded by University of Queensland on 1/21/2019 6:03:50 AM.

Table 3 Concentration of atoms at the original surface and at a 10.0 nm depth of silver deposit measured by XPS (units of atom%)

| | Ag 3d (%) | C 1s (%) | O 1s (%) | N 1s (%) | S 2p (%) |
|---|---|---|---|---|---|
| No etching | 54.06 | 34.27 | 3.93 | 7.74 | 0 |
| Etching 2 min | 74.87 | 25.13 | 0 | 0 | 0 |

The surface adsorption of DMH or NA did not influence the conductivity of the bulk silver, since the surface adsorption layer was only a single molecular layer. Thus, the silver deposit obtained from the introduced bath could be used in microelectronics, aerospace, automotive, and jewelry applications, due to its high purity and electrical properties.

### 3.6 Conductivity of silver deposit

The conductivity of the silver deposit is a key function for the application in microelectronics. The contact resistance of silver deposits obtained from the introduced bath and from the conventional cyanide silver electroplating bath was studied with the same technique. The process was repeated up to five times for every deposit, with the results of the contact resistance measurements displayed in Table 4.

As shown in Table 4, the contact resistance of the silver deposit obtained from the introduced bath was smaller than that of the cyanide deposit. For application with electronics packaging, silver deposits with smaller contact resistance could significantly increase the service life of microelectronics. This indicated that the cyanide silver electroplating bath could be improved for application in microelectronics by replacing cyanide with the suggested bath.

### 3.7 Welding properties of silver deposit

To be applied in electronic packaging, the silver deposit should possess excellent welding properties with solder and connectors. The welding properties of prepared silver deposits were measured by a wire pull technique, as depicted in Fig. 11.

A gold wire with $d$ = 25 μm was used for the welding measurement of the silver deposit, with a pulling force of 80 gf. The process was repeated up to five times for every deposit, with Table 5 showing the measurement results of the silver deposit welding properties. The welding properties of the silver deposits obtained from the introduced bath were close to that of the cyanide bath silver deposit used in microelectronics for more than 100 years. In the welding property measurements, no break occurred in the welded joints (1st point and 2nd point), indicating that the introduced silver deposit can be used in microelectronics with high reliability. This shows that the introduced silver deposit, with an excellent welding property, can be used for electronic packaging to replace cyanide silver electroplating baths.

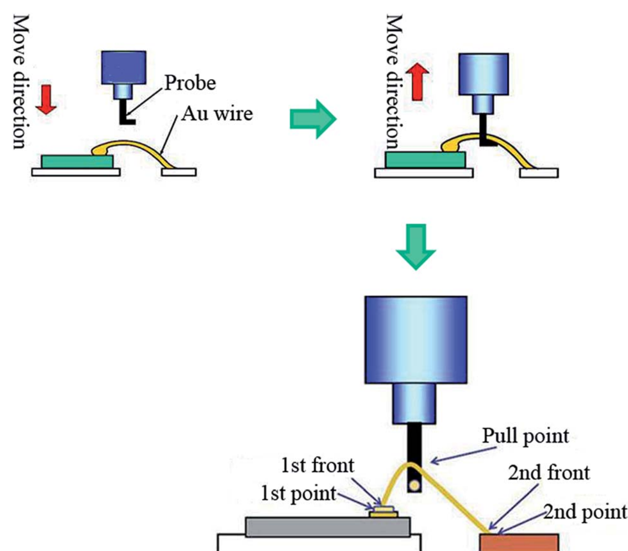


Fig. 11 Scheme of the welding property measurement.

Table 5 Welding properties of silver deposits obtained from different silver electroplating baths (units of gf)

| | Maximum | Minimum | Average | Variance |
|---|---|---|---|---|
| Introduced bath | 6.80 | 6.30 | 6.54 | 0.50 |
| Cyanide bath | 6.90 | 6.20 | 6.54 | 0.11 |

## 4. Conclusions

In summary, we report a novel method for predicting the behavior of complexing agents in mirror-bright silver electroplating processes, using quantum chemical calculations and molecular dynamic simulations. The results of the quantum chemical calculations suggest that DMH and NA could be used as potential complexing agents for silver electroplating, based on their electronic properties and orbital information. The results of the MD simulations showed that DMH and NA could adsorb onto the copper and silver surfaces strongly, leading to a higher inhibited effect for silver electrodeposition on the copper and silver surfaces.

Table 4 Contact resistances of silver deposits obtained from different silver electroplating baths (units of $10^{-4}$ Ω)

| | 10 gf | 20 gf | 30 gf | 40 gf | 50 gf | 60 gf | 70 gf | 80 gf | 90 gf | 100 gf |
|---|---|---|---|---|---|---|---|---|---|---|
| Introduced deposit | 8.2 | 6.2 | 5.0 | 4.6 | 4.2 | 3.8 | 3.4 | 3.2 | 3.0 | 3.0 |
| Cyanide deposit | 9.0 | 7.2 | 6.4 | 5.4 | 5.0 | 4.8 | 4.4 | 4.2 | 4.2 | 4.0 |


This journal is © The Royal Society of Chemistry 2014

Published on 18 August 2014. Downloaded by University of Queensland on 1/21/2019 6:03:50 AM.

Silver(I)-complexes in the proposed bath possessed good complex stability, with no displacement reactions occurring between the silver plating bath and the copper, indicating a promising, efficient procedure that can omit the strike-plating process. A mirror-bright silver deposit with excellent leveling capability, smooth and compact morphologies, and high purity and conductivity, as well as excellent welding properties could be obtained from the introduced bath without any additives.

The plating bath, containing DMH and NA as complexing agents for silver electrodeposition, is innovative, simple, stable and environmentally friendly with low toxicity and an ease of disposal. Furthermore, the excellent properties of the resulting silver deposits render this plating bath arrangement as a highly promising replacement for the conventional cyanide silver electroplating baths commonly used in the microelectronics industry.

## Acknowledgements

Financial support from the State Key Laboratory of Urban Water Resource and Environment (Harbin Institute of Technology) (2012DX03) for this work is gratefully acknowledged.

## References

1 Z. S. Pereira and E. Z. da Silva, *J. Phys. Chem. C*, 2011, **115**, 22870–22876.
2 R. Zhang, W. Lin, K. Lawrence and C. P. Wong, *Int. J. Adhes. Adhes.*, 2010, **30**, 403–407.
3 W. Zhao, Y. Liu, J. Liu, P. Chen, I. W. Chen, F. Huang and J. Lin, *J. Mater. Chem. A*, 2013, **1**, 7942–7948.
4 R. Zhang, W. Lin, K. S. Moon and C. P. Wong, *ACS Appl. Mater. Interfaces*, 2010, **2**, 2637–2645.
5 P. Peng, A. Hu, H. Huang, A. P. Gerlich, B. Zhao and Y. N. Zhou, *J. Mater. Chem.*, 2012, **22**, 12997–13001.
6 J. Wang, Z. Chen, Y. Hu, X. Jiang, D. Chen and W. Zhang, *J. Mater. Chem. C*, 2013, **1**, 230–233.
7 K. Márquez, G. Staikov and J. W. Schultze, *Electrochim. Acta*, 2003, **48**, 875–882.
8 B. C. Baker, M. Freeman, B. Melnick, D. Wheeler, D. Josell and T. P. Moffat, *J. Electrochem. Soc.*, 2003, **150**, C61–C66.
9 B. Bozzini, L. D'Urzo, C. Mele and V. Romanello, *J. Phys. Chem. C*, 2008, **112**, 6352–6358.
10 S. A. Hossain and M. Saitou, *J. Appl. Electrochem.*, 2008, **38**, 1653–1657.
11 G. Baltrūnas, *Electrochim. Acta*, 2003, **48**, 3659–3664.
12 R. Bomparola, S. Caporali, A. Lavacchi and U. Bardi, *Surf. Coat. Technol.*, 2007, **201**, 9485–9490.
13 Y. B. Patil and K. M. Paknikar, *Lett. Appl. Microbiol.*, 2000, **30**, 33–37.
14 C. L. Lasko and M. P. Hurst, *Environ. Sci. Technol.*, 1999, **33**, 3622–3626.
15 D. G. Foster, Y. Shapir and J. Jorne, *J. Electrochem. Soc.*, 2005, **152**, C462–C465.
16 D. G. Foster, Y. Shapir and J. Jorné, *J. Electrochem. Soc.*, 2003, **150**, C375–C380.
17 D. Gonnissen, S. Vandeputte, A. Hubin and J. Vereecken, *Electrochim. Acta*, 1996, **41**, 1051–1056.
18 S. Vandeputte, A. Hubin and J. Vereecken, *Electrochim. Acta*, 1997, **42**, 3429–3441.
19 B.-G. Xie, J.-J. Sun, Z.-B. Lin and G.-N. Chen, *J. Electrochem. Soc.*, 2009, **156**, D79–D83.
20 M. Miranda-Hernández and I. González, *J. Electrochem. Soc.*, 2004, **151**, C220–C228.
21 B. J. Polk, M. Bernard, J. J. Kasianowicz, M. Misakian and M. Gaitan, *J. Electrochem. Soc.*, 2004, **151**, C559–C566.
22 B. Reents, W. Plieth, V. Macagno and G. Lacconi, *J. Electroanal. Chem.*, 1998, **453**, 121–127.
23 G. M. Oliveira, M. R. Silva and I. A. Carlos, *J. Mater. Sci.*, 2007, **42**, 10164–10172.
24 Z.-B. Lin, B.-G. Xie, J.-S. Chen, J.-J. Sun and G.-N. Chen, *J. Electroanal. Chem.*, 2009, **633**, 207–211.
25 Z.-B. Lin, J.-H. Tian, B.-G. Xie, Y.-A. Tang, J.-J. Sun, G.-N. Chen, B. Ren, B.-W. Mao and Z.-Q. Tian, *J. Phys. Chem. C*, 2009, **113**, 9224–9229.
26 M.-C. Tsai, D.-X. Zhuang and P.-Y. Chen, *Electrochim. Acta*, 2010, **55**, 1019–1027.
27 S. J. Zhou, D. L. Preston, P. S. Lomdahl and D. M. Beazley, *Science*, 1998, **279**, 1525–1527.
28 M. E. Tuckerman, D. Marx, M. L. Klein and M. Parrinello, *Science*, 1997, **275**, 817–820.
29 K. Honkala, A. Hellman, I. N. Remediakis, A. Logadottir, A. Carlsson, S. Dahl, C. H. Christensen and J. K. Norskov, *Science*, 2005, **307**, 555–558.
30 H. Li, Y. Li and M. Chen, *RSC Adv.*, 2013, **3**, 12133–12139.
31 S. Bhattacharyya and K. Hatua, *RSC Adv.*, 2014, **4**, 18702–18709.
32 H. Monajemi, M. H. Cheah, V. S. Lee, S. M. Zain and W. A. Tajuddin Wan Abdullah, *RSC Adv.*, 2014, **4**, 10505–10513.
33 D. V. Deubel and T. Ziegler, *Organometallics*, 2002, **21**, 1603–1611.
34 M. K. Nazeeruddin, F. De Angelis, S. Fantacci, A. Selloni, G. Viscardi, P. Liska, S. Ito, B. Takeru and M. Grätzel, *J. Am. Chem. Soc.*, 2005, **127**, 16835–16847.
35 K. K. Paulla, A. J. Hassan, C. R. Knick and A. A. Farajian, *RSC Adv.*, 2014, **4**, 2346–2354.
36 Z. Zhang, K. Yan and J. Zhang, *RSC Adv.*, 2013, **3**, 6401–6407.
37 C.-Y. Chang, S.-P. Ju, J.-W. Chang, S.-C. Huang and H.-W. Yang, *RSC Adv.*, 2014, **4**, 26074.
38 J. Vatamanu, O. Borodin, D. Bedrov and G. D. Smith, *J. Phys. Chem. C*, 2012, **116**, 7940–7951.
39 G. A. Pereira, A. C. Massabni, E. E. Castellano, L. A. S. Costa, C. Q. F. Leite, F. R. Pavan and A. Cuin, *Polyhedron*, 2012, **38**, 291–296.
40 L. Zhang, A. Fonari, Y. Zhang, G. Zhao, V. Coropceanu, W. Hu, S. Parkin, J.-L. Brédas and A. L. Briseno, *Chem.–Eur. J.*, 2013, **19**, 17907–17916.
41 T. Jurca, S. Ouanounou, S. I. Gorelsky, I. Korobkov and D. S. Richeson, *Dalton Trans.*, 2012, 4765–4771.
42 A. Groß, F. Gossenberger, X. Lin, M. Naderian, S. Sakong and T. Roman, *J. Electrochem. Soc.*, 2014, **161**, E3015–E3020.

View Article Online


Published on 18 August 2014. Downloaded by University of Queensland on 1/21/2019 6:03:50 AM.


43 D. H. Brouwer, I. L. Moudrakovski, R. J. Darton and R. E. Morris, *Magn. Reson. Chem.*, 2010, **48**, S113–S121.
44 J. Zhang, Z. He, W. Li and Y. Han, *RSC Adv.*, 2012, **2**, 4814–4821.
45 S. Meng, Y. Tang, Y. Yin, X. Yin and J. Xie, *RSC Adv.*, 2013, **3**, 18115–18127.
46 B. Honarparvar, T. Govender, G. E. Maguire, M. E. Soliman and H. G. Kruger, *Chem. Rev.*, 2014, **114**, 493–537.
47 M. L. Klein and W. Shinoda, *Science*, 2008, **321**, 798–800.
48 H. Chermette, *Coord. Chem. Rev.*, 1998, **178–180**, 699–721.
49 G. Harrach, Z. Valicsek and O. Horváth, *Inorg. Chem. Commun.*, 2011, **14**, 1756–1761.
50 C. I. Maxwell, A. A. Neverov, N. J. Mosey and R. Stan Brown, *J. Phys. Org. Chem.*, 2014, **27**, 419–429.
51 H. Wang, N. J. D. Yonker, H. Gao, C. Tan, X. Zhang, L. Ji, C. Zhao and Z.-W. Mao, *RSC Adv.*, 2012, **2**, 436–446.
52 W. F. van Gunsteren and H. J. Berendsen, *Angew. Chem., Int. Ed.*, 1990, **29**, 992–1023.
53 O. Lopez-Acevedo, K. A. Kacprzak, J. Akola and H. Häkkinen, *Nat. Chem.*, 2010, **2**, 329–334.
54 T. Duren, Y. S. Bae and R. Q. Snurr, *Chem. Soc. Rev.*, 2009, **38**, 1237–1247.
55 T. P. Brennan, J. T. Tanskanen, J. R. Bakke, W. H. Nguyen, D. Nordlund, M. F. Toney, M. D. McGehee, A. Sellinger and S. F. Bent, *Chem. Mater.*, 2013, **25**, 4354–4363.
56 A. Kornherr, S. Hansal, W. E. G. Hansal, J. r. O. Besenhard, H. Kronberger, G. E. Nauer and G. Zifferer, *J. Chem. Phys.*, 2003, **119**, 9719–9728.
57 A. Kornherr, G. E. Nauer, A. A. Sokol, S. A. French, C. R. A. Catlow and G. Zifferer, *Langmuir*, 2006, **22**, 8036–8042.
58 C. Wang, M. An, P. Yang and J. Zhang, *Electrochem. Commun.*, 2012, **18**, 104–107.
59 C. Wang, J. Zhang, P. Yang and M. An, *Electrochim. Acta*, 2013, **92**, 356–364.
60 J. Zhang, G. Qiao, S. Hu, Y. Yan, Z. Ren and L. Yu, *Corros. Sci.*, 2011, **53**, 147–152.
61 S. Xia, M. Qiu, L. Yu, F. Liu and H. Zhao, *Corros. Sci.*, 2008, **50**, 2021–2029.
62 M. Meusel and M. Gütschow, *Org. Prep. Proced. Int.*, 2004, **36**, 391–443.
63 M. Puszyńska-Tuszkanow, T. Grabowski, M. Daszkiewicz, J. Wietrzyk, B. Filip, G. Maciejewska and M. Cieślak-Golonka, *J. Inorg. Biochem.*, 2011, **105**, 17–22.
64 K. Oyaizu, Y. Ohtani, A. Shiozawa, K. Sugawara, T. Saito and M. Yuasa, *Inorg. Chem.*, 2005, **44**, 6915–6917.
65 G. Z. Pavlovich and R. G. Luthy, *Water Res.*, 1988, **22**, 327–336.
66 X. W. Yang, M. Z. An, Y. W. Zhang and L. Zhang, *Electrochim. Acta*, 2011, **58**, 516–522.
67 S. El Issami, L. Bazzi, M. Mihit, B. Hammouti, S. Kertit, E. A. Addi and R. Salghi, *Pigm. Resin Technol.*, 2007, **36**, 161–168.
68 K. Barouni, L. Bazzi, R. Salghi, M. Mihit, B. Hammouti, A. Albourine and S. El Issami, *Mater. Lett.*, 2008, **62**, 3325–3327.


 This journal is © The Royal Society of Chemistry 2014